Designing Responsive Buckled Surfaces by Halftone Gel Lithography

Jungwook Kim, *et al.*

Science **335**, 1201 (2012);
DOI: 10.1126/science.1215309

Science (print ISSN 0036-8075; online ISSN 1095-9203) is published weekly, except the last week in December, by the American Association for the Advancement of Science, 1200 New York Avenue NW, Washington, DC 20005.

Designing Responsive Buckled Surfaces by Halftone Gel Lithography

Jungwook Kim,[1] James A. Hanna,[2] Myunghwan Byun,[1] Christian D. Santangelo,[2]* Ryan C. Hayward[1]*

Self-actuating materials capable of transforming between three-dimensional shapes have applications in areas as diverse as biomedicine, robotics, and tunable micro-optics. We introduce a method of photopatterning polymer films that yields temperature-responsive gel sheets that can transform between a flat state and a prescribed three-dimensional shape. Our approach is based on poly(*N*-isopropylacrylamide) copolymers containing pendent benzophenone units that allow cross-linking to be tuned by irradiation dose. We describe a simple method of halftone gel lithography using only two photomasks, wherein highly cross-linked dots embedded in a lightly cross-linked matrix provide access to nearly continuous, and fully two-dimensional, patterns of swelling. This method is used to fabricate surfaces with constant Gaussian curvature (spherical caps, saddles, and cones) or zero mean curvature (Enneper's surfaces), as well as more complex and nearly closed shapes.

Soft materials are ideal for designing structures that reversibly change shape in response to stimuli. Techniques for fabricating and actuating responsive structures include swelling of patterned gels (*1*–*4*) and electroactive polymers (*5*), light-induced switching of liquid-crystal elastomers (*6*–*8*), actuation of dielectric elastomers on rigid frames (*9*), recovery of shape-memory polymers (*10*), and growth of muscle cells on compliant polymeric supports (*11*). An approach with great potential for the design of complex actuating structures is the buckling of thin sheets into three-dimensional (3D) shapes induced by spatially nonuniform growth, a common motif in biological morphogenesis (*12*–*16*). Because bending is less costly than compression for thin sheets, the nonuniform stresses developed as a result of patterned growth are relieved by out-of-plane deformation. Nevertheless, fundamental questions remain to be answered before this principle can be used as a practical means to form precise 3D structures. Chief among these is our incomplete understanding of how in-plane stresses translate to 3D shapes. Although nonuniform swelling is connected geometrically to Gaussian curvature (*17*), bending elasticity typically still plays an important role in determining the final structure (*18*, *19*). Surprisingly, some swelling patterns that should provide constant negative Gaussian curvature lead to wrinkling, even though they are not geometrically required to do so (*17*). In addition, swelling patterns exist for which in-plane stresses cannot be completely relieved by buckling; in such cases, the resulting shapes remain largely unexplored.

Efforts to understand shaping driven by nonuniform growth and to translate these principles into practical strategies for controlling the shapes of thin sheets were inspired nearly a decade ago by studies of the buckling of torn plastic sheets (*20*). More recently, Sharon and co-workers (*17*) developed a method wherein temporal control over the composition of a monomer solution introduced into a Hele-Shaw cell was used to write patterns in the shrinkage of a thermally responsive gel. Though an elegant step toward the design of materials with structures defined by patterned growth, this approach is limited to profiles that vary in only one direction, fundamentally restricting the 3D configurations that can be accessed. Thus, the need for strategies to print truly arbitrary patterns of expansion or contraction in synthetic materials has remained a central challenge for the field (*21*).

Here, we describe a solution to this challenge through an approach we call "halftone gel lithography," based on a simple two-mask lithographic patterning of photo-cross-linkable copolymer films. Even though the halftone swelling patterns yield in-plane stresses that cannot be eliminated entirely, we find that sufficiently thick sheets smooth out these sharp transitions and yield predictable 3D shapes. This method enables the prescription of effectively smooth swelling profiles on thin sheets with arbitrary 2D geometries, thereby providing access to complex 3D structures. This work opens the door not only to addressing fundamental questions surrounding growth-induced shaping of thin sheets but also to practical fabrication of responsive gel microdevices based on the principles of nonuniform growth.

Our method relies on a temperature-responsive *N*-isopropylacrylamide (NIPAm) copolymer containing photo-cross-linkable benzophenone (*22*) acrylamide (BPAm) units (Fig. 1A). Acrylic acid (AAc) comonomers are included to increase hydrophilicity, and rhodamine B methacrylate (RhBMA) facilitates imaging by fluorescence microscopy. Cross-linking is achieved by exposure of solution-cast copolymer films (with dry thicknesses $h \approx 7$ to 17 μm) to ultraviolet (UV) light (~360 nm), which activates the benzophenone units to form covalent cross-links between polymer chains. The key to spatially patterned swelling is that the conversion of BPAm to cross-links, and therefore the swelling of the material, can be tuned through the dose of UV. We characterize the material in terms of the equilibrium areal swelling ratio Ω, defined as the ratio of the area of a homogeneous film in the fully swelled state in aqueous solution (1 mM NaCl, 1 mM phosphate buffer; pH 7.2) to the area in the dry, as-cross-linked state. As shown in fig. S1, a small dose of UV light (0.2 J/cm^2) is sufficient to gel the polymer film and gives rise to the highest achievable swelling ratio of $\Omega_{high} = 8.2$ at 22°C, whereas maximum conversion of BPAm at a much larger dose (13.9 J/cm^2) leads to materials with substantially reduced swelling, $\Omega_{low} = 2.3$ at 22°C.

This material system provides considerable flexibility for generating swelling patterns on thin elastic sheets. Using traditional photomasks with high contrast between opaque and nearly transparent regions, a series of n different masks aligned in succession allows any region of the sheet to receive one of 2^n distinct irradiation doses. In some cases, simple patterns consisting of only a few discrete levels of swelling may be adequate to achieve the desired control of shape; however, this scenario is poorly understood compared to that of plates with smoothly varying metrics. The use of a large number of masks would allow for fine gradations in swelling, presumably allowing smooth metrics to be approximated, with the drawback that an increased number of mask alignment steps makes the process more difficult and less robust. Alternatively, true "grayscale" lithographic techniques could be employed to provide nearly continuous variations in light intensity through masked or maskless exposures, but these methods require complex lithographic processes or mask fabrication steps (*23*, *24*).

Instead, we focus on a simple approach inspired by the ubiquitous printing method of halftoning, wherein continuous variations in tone are simulated using only a few colors of ink. The process of halftone gel lithography is illustrated in Fig. 1, B to G. An initial photomask is used to define the overall shape of the object by providing a small dose of UV light that sets the swelling of the material to Ω_{high}. A second mask is used to define a pattern of circular dots of diameter d that are extensively cross-linked to restrict their swelling to Ω_{low}. We use a hexagonal lattice of dots with a lattice spacing a that is held constant on any given sheet, while d is varied in space, thus allowing nearly continuous changes in swelling to be printed in 2D. Whereas traditional halftone printing takes advantage of the

[1]Polymer Science and Engineering, University of Massachusetts, Amherst, MA 01003, USA. [2]Department of Physics, University of Massachusetts, Amherst, MA 01003, USA.

*To whom correspondence should be addressed. E-mail: csantang@physics.umass.edu (C.D.S.); rhayward@mail.pse.umass.edu (R.C.H.)

limited resolution of the human eye to provide the illusion of a homogeneous tone from closely spaced dots, our approach relies on the elasticity of the thin polymer sheet to locally smooth out the sharp contrast between the highly cross-linked dots and lightly cross-linked matrix, thereby yielding an intermediate degree of swelling.

To calibrate the method, we first explore the swelling of disks with dots of uniform diameter. As indicated in Fig. 1H, these disks show globally homogeneous swelling by an amount Ω that can be continuously tuned between the two extremes Ω_{low} and Ω_{high} by changing the area fraction of low-swelling regions, defined for $d \leq a$ as

$$\phi_{low} = \frac{\pi}{2\sqrt{3}}\left(\frac{d}{a}\right)^2 \quad (1)$$

Given that Ω is largely insensitive to ϕ_{low} beyond the point when neighboring dots begin to touch—that is, at $\phi_{low} \geq 0.91$—for simplicity we restrict dot sizes to $d \leq a$ without appreciably restricting the accessible range of swelling.

A simple model to describe swelling comes from considering the two gel regions as lumped 1D elements in parallel [see the supporting online material (SOM) for details], yielding the prediction

$$\frac{\phi_{low} + \alpha(1-\phi_{low})}{\Omega^{1/2}} = \frac{\phi_{low}}{\Omega_{low}^{1/2}} + \frac{\alpha(1-\phi_{low})}{\Omega_{high}^{1/2}} \quad (2)$$

where α is the ratio of the elastic moduli in the two material regions. Although this model captures the essential qualitative physics of mutually constrained swelling, it is too simple to yield quantitative agreement with material properties; thus, in practice α is treated as a fitting parameter. As shown in Fig. 1H, a value of $\alpha = 0.56$ provides a good fit to the observed swelling of halftoned composite gels. As expected based on the well-known temperature sensitivity of NIPAm copolymers, at each value of ϕ_{low} the composite disks deswell with increasing temperature, as shown in Fig. 1I. However, since the lightly cross-linked regions show more pronounced deswelling, the values of swelling converge to a narrow range between 1 and 2 at 45° to 50°C.

Whereas the composite disks described in Fig. 1 behave as homogeneous materials on length scales longer than the lattice dimension, the compressive stresses present in the lightly cross-linked matrix may cause local buckling when the disks are made sufficiently thin. To prevent this, we expect that the length scale of the lattice should not be much larger than h. Indeed, when we vary the dot size and spacing at constant $\phi_{low} = 0.4$, we find a critical lattice spacing, $a_c = (7.9 \pm 0.8)h$, below which the sheets remain flat and above which the high-swelling regions form buckled ridges spanning neighboring dots (Fig. 1J). Although the prefactor relating a_c and h will depend somewhat on ϕ_{low}, for the remainder of the discussion we will keep $a \leq 4h$, which is sufficient to avoid local buckling in all cases.

Having established that halftoning provides access to nearly continuous variations in swelling for disks with homogeneous dot sizes, we next consider the printing of spatially varying, axisymmetric, patterns of growth corresponding to target shapes with constant Gaussian curvature K, as shown in Fig. 2, A to D. Following Sharon and co-workers (*17*, *18*, *21*), we refer to $\Omega(\mathbf{r})$ as the "target metric" encoding the local equilibrium distances between points on the surface. A sheet of vanishing thickness should adopt the isometric embedding of this target metric with the lowest bending energy (*18*), provided that such an embedding exists. Written in terms of the coordinates on the flat, unswelled gel sheet, the target curvature at a material point $\mathbf{r}$ is set by the swelling factor $\Omega(\mathbf{r})$ according to Gauss's *theorema egregium*, $K = -\nabla^2 \ln\Omega/(2\Omega)$ (*25*). Thus, where r represents the radial position in a cylindrical coordinate system and c, R, and β are constants, swelling factors of the form

$$\Omega(r) = c\left(\frac{r}{R}\right)^{\beta} \quad (3)$$

should yield $K = 0$, whereas those of the form

$$\Omega(r) = \frac{c}{[1 + (r/R)^2]^2} \quad (4)$$

should yield constant $K = 4/(cR^2)$. Figure 2F shows four example metrics: a piece of a saddle surface with $K = -16.8$ mm^{-2}, a cone with an excess angle (*26*) specified by a swelling power-law exponent $\beta = 1$, a spherical cap with $K = 5.7$ mm^{-2}, and a cone with a deficit angle specified by $\beta = -0.4$. The corresponding patterns of dots were computed by evaluating the value

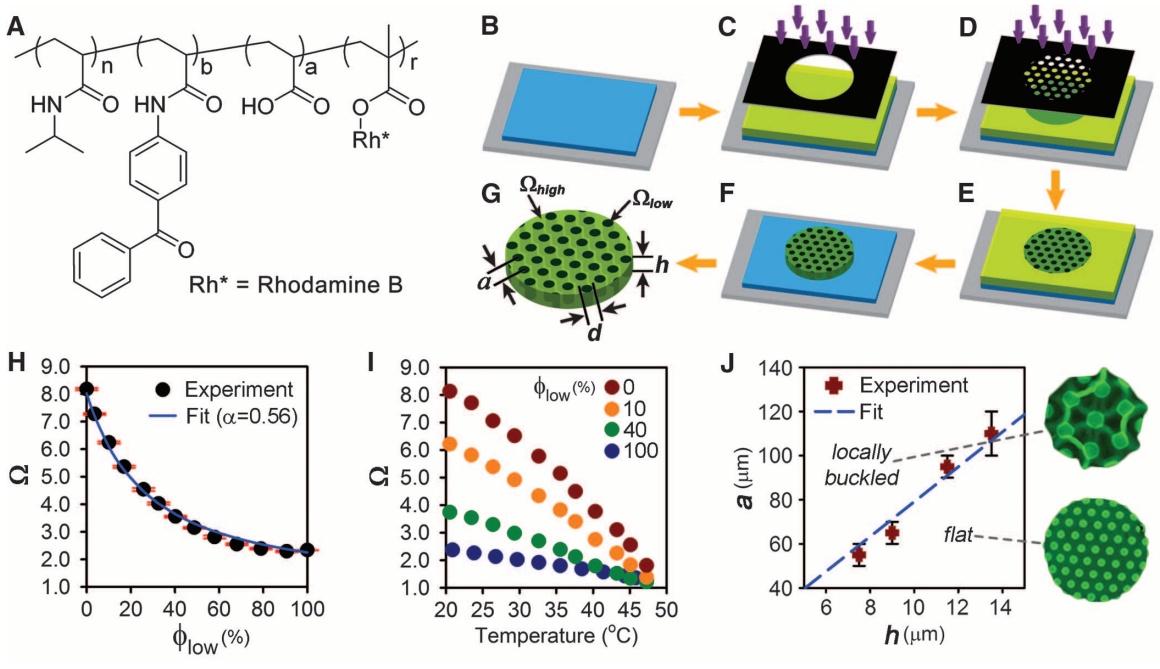

Fig. 1. Halftone gel lithography and characterization of composite disks. (**A**) Chemical structure of the photo-cross-linkable and temperature-responsive NIPAm copolymer. (**B** to **G**) A schematic illustration of halftone gel lithography. (B) On a silicon wafer coated with a sacrificial layer, (C) the copolymer film (thickness h = 7 to 17 μm) is solution-cast and exposed to a small dose of UV light through the first photomask and subsequently (D) a large dose through the second photomask. (E) The patterned film is (F) developed to remove uncross-linked material and (G) immersed in aqueous solution to release it from the substrate and induce swelling. (**H**) The areal expansion ratio Ω of composite disks at 22°C is plotted against the area fraction of dots ϕ_{low}. Experimental data (black solid circles) are fitted with Eq. 2 (blue line). The error bars denote standard deviations for six independent measurements. (**I**) The temperature dependence of Ω of the composite disks is shown for four different values of ϕ_{low}. (**J**) Below a thickness-dependent critical lattice spacing a_c, disks remain flat, whereas above a_c they undergo local buckling between neighboring dots. The value of a_c is plotted for a range of film thicknesses (symbols), along with a least squares fit of a linear relationship with zero intercept (dashed line).

of $\Omega(r)$ at each lattice point according to Eqs. 3 and 4, determining the corresponding value of ϕ_{low} from the fit of Eq. 2 to the data in Fig. 1H, and finally setting the size of the dot at that lattice point according to Eq. 1. Because the power-law metrics in Eq. 3 diverge or vanish at the origin, it is necessary to cut out a small region around the center of each of the two cones.

The shapes adopted by the corresponding gel sheets (Fig. 2, A to D) are measured by laser scanning confocal fluorescence microscopy (LSCM) and analyzed as described in the SOM. Each of the four surfaces shows only small deviations about an average Gaussian curvature, with the exception of the regions near the free edges, where our analysis yields artifactual curvatures (due to the finite thickness of the gel sheets, the surface meshing procedure used yields additional points on the edges that do not accurately reflect the 2D geometries of the sheets). After excluding regions of the surface within $2h$ of the edges to avoid these artifacts, we find the average Gaussian curvatures of the spherical cap and saddle to be 6.2 mm^{-2} and –20.6 mm^{-2}, respectively, with nearly axisymmetric distributions of curvature (fig. S2A). Both values are in reasonable agreement with the target values, although the tendency of disks with uniform dot sizes to show slight curvatures (with radii of 2 mm) suggests the presence of slight through-thickness variations in swelling (see SOM for details) that may contribute to the observed deviations from the programmed curvature. Interestingly, we do not observe a boundary layer with negative Gaussian curvature around the edge of the spherical cap as has been reported for truly smooth metrics (*17*, *18*), possibly reflecting the influence of the through-thickness variations in swelling. For both cones, the average Gaussian curvatures, excluding regions at the free edges, are close to zero. Further, Fig. 2E shows a plot of the deficit angle δ measured for five different cone metrics with power law exponents $-1 \le \beta < 0$, which agrees closely with the programmed value $\delta = -\pi\beta$.

We next consider metrics of the form

$$\Omega(r) = c[1 + (r/R)^{2(n-1)}]^2 \qquad (5)$$

corresponding to Enneper's minimal surfaces with n nodes. These surfaces all have zero mean curvature and so are expected to minimize the elastic energy for these metrics at vanishing thickness (*18*). Although Eq. 5 is axisymmetric, Enneper's surfaces spontaneously break axial symmetry by forming n wrinkles. In Fig. 2, G to J, we demonstrate patterned surfaces with n = 3 to 6, each of which reproduces the targeted number of wrinkles. As shown in the maps of curvature in Fig. 2 (and azimuthally averaged plots in fig. S2B), each surface has small mean curvature and negative Gaussian curvature that matches closely with the target profile. For a given film thickness, increasing n eventually leads to a saturation in the number of wrinkles, because the bending energy arising from Gaussian curvature increases with n (for the films with $h \approx 7$ μm in Fig. 4, a metric with $n = 8$ yielded only six wrinkles). However, given the subtle differences between the metrics plotted in Fig. 2F, the ability to accurately reproduce the programmed number of wrinkles for n = 3 to 6 is a strong testament to the fidelity of the metrics patterned by this technique.

The true power of our approach lies in the fabrication of nonaxisymmetric swelling patterns. As a simple demonstration, we first consider the problem of how to form a sphere through growth. For the axisymmetric metric described in Eq. 4, the maximum value of r/R to which this metric can be experimentally patterned is restricted by the accessible range of swelling. In our case, this range is $\Omega_{high}/\Omega_{low} \approx 3.7$, limiting the maximum portion of a sphere that can be obtained to slightly less than half. Although further improvements in the material system are likely to increase the available range, the axisymmetric metric is inherently an inefficient way to form a sphere, because as one seeks to go beyond a hemisphere and toward a closed shape, the required swelling contrast diverges rapidly. Given access to 2D metrics, however, a number of well-established conformal mappings of the sphere onto flat surfaces are known from the field of map projections. For example, the Peirce quincuncial projection (*27*) maps a sphere of radius R onto a square using the metric

$$\Omega(x,y) = 2\frac{\left|dn\left(\frac{x+iy}{R}\middle|\frac{1}{\sqrt{2}}\right)sn\left(\frac{x+iy}{R}\middle|\frac{1}{\sqrt{2}}\right)\right|^2}{\left[1+\left|cn\left(\frac{x+iy}{R}\middle|\frac{1}{\sqrt{2}}\right)\right|^2\right]^2} \qquad (6)$$

where sn, cn, and dn are Jacobi elliptic functions, and x and y are the components of $\mathbf{r}$. This metric still has four cusp-like singularities where $\Omega(\mathbf{r}) = 0$; however, one of its useful properties as a map projection is that only a small portion

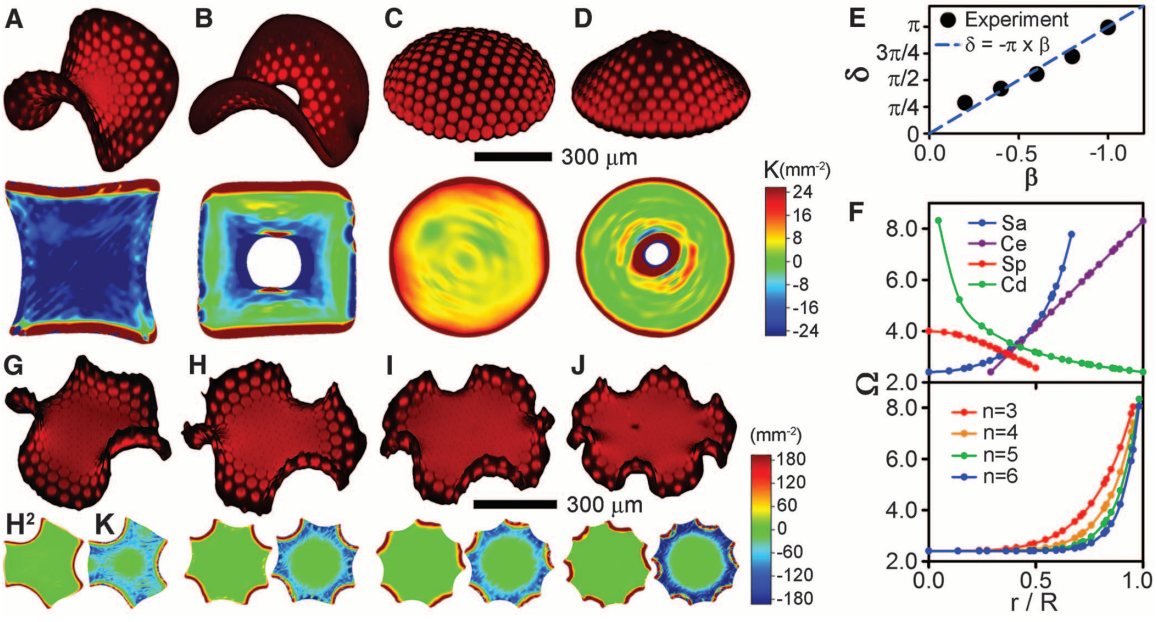

Fig. 2. Halftoned disks with axisymmetric metrics. Patterned sheets programmed to generate (**A**) a piece of saddle surface (Sa), (**B**) a cone with an excess angle (Ce), (**C**) a spherical cap (Sp), and (**D**) a cone with a deficit angle (Cd). (Top) 3D reconstructed images of swollen hydrogel sheets and (bottom) top-view surface plots of Gaussian curvature. Initial thicknesses and disk diameters are 9 and 390 μm, respectively, although the apparent thickness of sheets is enlarged due to the resolution of the LSCM. (**E**) Measured values of deficit angle δ for cones with five different exponents β (see Eq. 3) (black solid circles) and the programmed values (blue dashed line). (**F**) Swelling factors for the target metrics as a function of normalized radial position on the unswelled disks r/R, with points plotted at values corresponding to lattice points to indicate the resolution with which Ω is patterned. (**G** to **J**) Patterned sheets programmed to generate Enneper's minimal surfaces with n = (G) 3, (H) 4, (I) 5, and (J) 6 wrinkles upon swelling as dictated by Eq. 5. 3D reconstructed images (top) and top-view surface plots of squared mean curvature H^2 and Gaussian curvature K (bottom). Initial thicknesses and disk diameters are 7 and 390 μm, respectively.

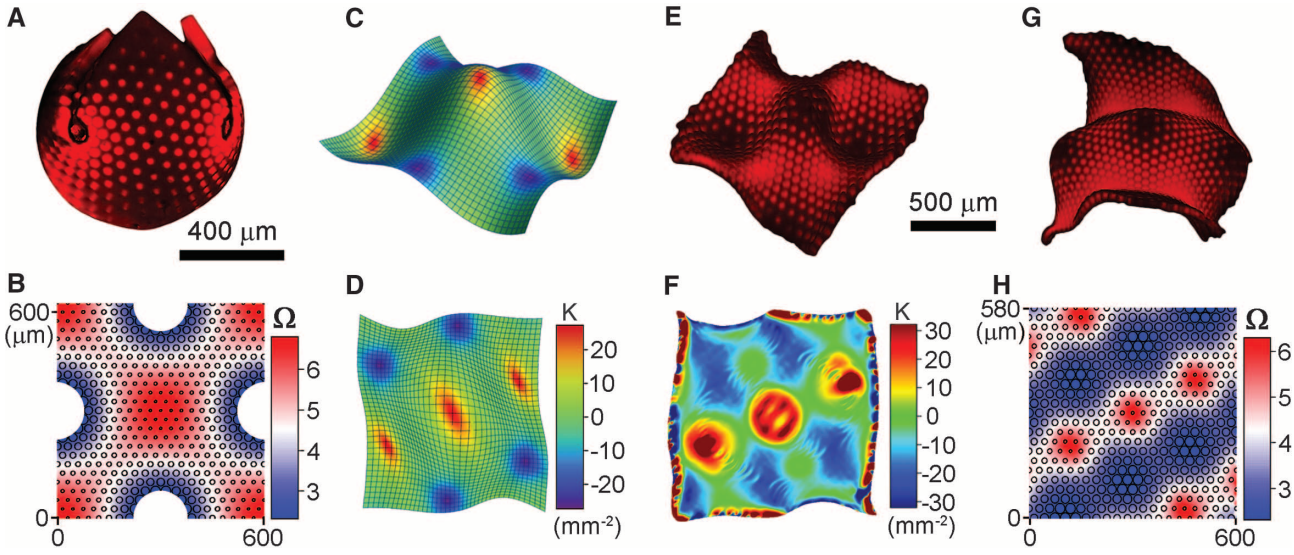

Fig. 3. Nonaxisymmetric swelling patterns. (**A**) A 3D reconstructed image of the nearly closed spherical shape formed by the metric of Eq. 6 and shown in (**B**); the sizes and positions of open circles correspond to those of the low-swelling dots. Before swelling, the patterned gel sheet was 9 μm thick, with lateral dimensions of 600 by 620 μm. (**C**) The target height profile of the corrugated surface, also shown in (**D**) top view. The grid represents the coordinate lines of the conformal coordinate system. (**E**) 3D reconstructed image and (**F**) Gaussian curvature of the sheet swollen into a shape similar to the target surface. (**G**) 3D reconstructed image of the shape adopted when each of the three regions of positive curvature along the center diagonal buckle in the same direction. (**H**) The swelling pattern used to generate sheets in (E) to (G). The sizes and positions of open circles correspond to those of the low-swelling dots. Before swelling, the patterned gel sheets were 9 μm thick and had lateral dimensions of 600 by 580 μm.

of the area of the sphere requires large distortions. Thus, we can approximate the metric by excising the small regions of the square where Ω falls below the experimentally accessible range, as shown in Fig. 3B. The resulting swelled shape (Fig. 3A) does indeed approximate that of a sphere (see fig. S3 for plots of surface curvatures) with four small regions removed, although the four corners of the square do not quite close. The reason for the latter behavior remains under investigation but may arise from the excised singularities and/or the finite bending energy of the sheet. Nonetheless, the contrast between the nearly closed shape achieved in Fig. 3A and the limited spherical caps that may be obtained for the same material system with an axisymmetric metric highlights the importance of 2D patterning, even for generating axisymmetric shapes.

Beyond fabricating simple shapes with constant target Gaussian curvature, our approach opens the door to shapes of arbitrary complexity. Although numerous fundamental questions and practical challenges remain to establishing the necessary design rules, we take a first step toward the construction of shapes whose swelling factors are not known a priori by considering a corrugated surface (Fig. 3C) described by the height function $H(x,y) = H_0 [\cos(2\pi x/L) + \cos(\pi x/L + \sqrt{3}\pi y/L)]$, where $2L$ is the width of the sheet. We choose H_0 = 60 μm and L = 300 μm. Determining an appropriate swelling factor is equivalent to finding a conformal coordinate system on the surface (as described in the SOM) and yields the swelling function shown in Fig. 3H. This example highlights some of the remaining challenges in designing arbitrary 3D shapes, because sheets patterned according to Fig. 3H often fail to form the desired shape upon swelling. The three local maxima in growth, lying along the line cutting diagonally through the center of the sheet, each represent regions of positive target Gaussian curvature; however, each may achieve its desired local curvature by buckling either upward or downward. Indeed, rather than buckling in the manner described by $H(x,y)$, these local maxima in swelling may instead all buckle in the same direction, as shown in Fig. 3G (again, possibly reflecting a preference for buckling in one direction due to slight through-thickness variations in swelling). However, in some cases, the sheets do swell into the corrugated conformation shown in Fig. 3E, which is very similar to the programmed surface $H(x,y)$, as can also be seen by comparing the targeted (Fig. 3D) and measured (Fig. 3F) Gaussian curvatures. The use of a glass micropipette to hold the patterned sheet against the substrate during swelling (upon cooling from 40° to 22°C) tends to constrain the sheet to swell into the corrugated shape, and initially misfolded sheets can also be "snapped through" into the desired configuration by application of force to the center-most region of positive curvature. Thus, we conclude that such surfaces with complex swelling patterns may in general form multiple different shapes that are locally metastable and that additional constraints may therefore be required to ensure that a specific shape is chosen.

Finally, we demonstrate the responsiveness of the patterned sheets to changes in temperature using another nonaxisymmetric metric that combines that for an Enneper's surface with four

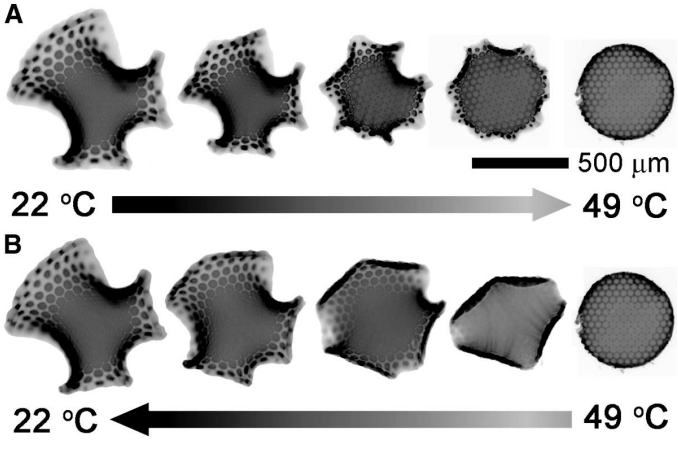

Fig. 4. Thermal actuation of patterned sheets. (**A**) When the temperature of the aqueous medium is increased, the hybrid Enneper's surface deswells and recovers its flat shape by 49°C. (**B**) Upon lowering the temperature to 22°C, the disk swells back to the initial hybrid shape through a different pathway. Initial thickness and disk diameter are 7 and 390 μm, respectively.

nodes along $0 < \theta < \pi$ with that for an Enneper's surface with two nodes along $\pi < \theta < 2\pi$. Remarkably, despite the sharp changes in the metric at $\theta = 0$ and π, the sheet does adopt the desired hybrid shape when swelled at room temperature, as shown in Fig. 4 (and as a movie in the SOM). As temperature is increased, Ω_{high} and Ω_{low} both decrease, but also converge, causing the buckled disc to first decrease in size and eventually flatten by 49°C. A subsequent decrease in temperature to 22°C causes the disc to regain its initial shape, although the progression of intermediate shapes is not the same. A more detailed study of the pathways and kinetics of swelling and deswelling is an interesting subject for future study.

In conclusion, we have demonstrated a simple method for halftone lithography of photo-cross-linkable copolymers that permits fabrication of stimulus-responsive gel sheets with micrometer-scale thicknesses and 2D patterned swelling. As long as the dots used to define the halftone pattern are smaller than several times the film thickness, the material behaves as a homogeneous elastic composite on length scales larger than the dot pattern. By patterning spatial variations in dot size, the degree of swelling of the composite gel sheets can be tuned effectively continuously across a wide range using only two high-contrast photomasks. This method provides access not only to simple radially symmetric metrics that yield shapes with nearly constant Gaussian curvature or almost zero mean curvature but also to truly 2D patterns of swelling. Thus, it represents a powerful method for fabricating stimuli-responsive gel micro-devices and studying fundamental questions about how 3D shapes are formed through differential growth in 2D.

References and Notes

1. Z. B. Hu, X. M. Zhang, Y. Li, *Science* **269**, 525 (1995).
2. J. R. Howse *et al.*, *Nano Lett.* **6**, 73 (2006).
3. B. Kaehr, J. B. Shear, *Proc. Natl. Acad. Sci. U.S.A.* **105**, 8850 (2008).
4. G. H. Kwon *et al.*, *Small* **4**, 2148 (2008).
5. E. W. H. Jager, E. Smela, O. Inganäs, *Science* **290**, 1540 (2000).
6. T. Ikeda, M. Nakano, Y. Yu, O. Tsutsumi, A. Kanazawa, *Adv. Mater. (Deerfield Beach Fla.)* **15**, 201 (2003).
7. M. Camacho-Lopez, H. Finkelmann, P. Palffy-Muhoray, M. Shelley, *Nat. Mater.* **3**, 307 (2004).
8. T. J. White *et al.*, *Soft Matter* **4**, 1796 (2008).
9. G. Kofod, W. Wirges, M. Paajanen, S. Bauer, *Appl. Phys. Lett.* **90**, 081916 (2007).
10. A. Lendlein, H. Jiang, O. Jünger, R. Langer, *Nature* **434**, 879 (2005).
11. A. W. Feinberg *et al.*, *Science* **317**, 1366 (2007).
12. P. B. Green, *Int. J. Plant Sci.* **153**, (S3), S59 (1992).
13. U. Nath, B. C. W. Crawford, R. Carpenter, E. Coen, *Science* **299**, 1404 (2003).
14. E. Sharon, M. Marder, H. L. Swinney, *Am. Sci.* **92**, 254 (2004).
15. J. Dervaux, M. Ben Amar, *Phys. Rev. Lett.* **101**, 068101 (2008).
16. H. Liang, L. Mahadevan, *Proc. Natl. Acad. Sci. U.S.A.* **108**, 5516 (2011).
17. Y. Klein, E. Efrati, E. Sharon, *Science* **315**, 1116 (2007).
18. E. Efrati, E. Sharon, R. Kupferman, *Phys. Rev. E Stat. Nonlin. Soft Matter Phys.* **80**, 016602 (2009).
19. M. A. Dias, J. A. Hanna, C. D. Santangelo, *Phys. Rev. E Stat. Nonlin. Soft Matter Phys.* **84**, 036603 (2011).
20. E. Sharon, B. Roman, M. Marder, G.-S. Shin, H. L. Swinney, *Nature* **419**, 579 (2002).
21. E. Sharon, E. Efrati, *Soft Matter* **6**, 5693 (2010).
22. R. Toomey, D. Freidank, J. Rühe, *Macromolecules* **37**, 882 (2004).
23. Z. Cui, J. Du, Y. Gu, *Proc. SPIE* **4984**, 111 (2003).
24. L. Erdmann, A. Deparnay, G. Maschke, M. Längle, R. Brunner, *J. Microlith. Microfab.* **4**, 041601 (2005).
25. M. do Carmo, *Differential Geometry of Curves and Surfaces* (Prentice Hall, New York, 1976).
26. M. M. Müller, M. B. Amar, J. Guven, *Phys. Rev. Lett.* **101**, 156104 (2008).
27. C. S. Peirce, *Am. J. Math.* **2**, 394 (1879).

Acknowledgments: We acknowledge stimulating discussions with M. M. Müller and E. Sharon at the Aspen Center for Physics, where part of this work was done. This research was funded by the Army Research Office through W911NF-11-1-0080 and the National Science Foundation through DMR-0846582, and made use of facilities supported by the NSF Materials Research Science and Engineering Center at the University of Massachusetts (DMR-0747756) and NSF grant BBS-8714235.

Supporting Online Material

www.sciencemag.org/cgi/content/full/335/6073/1201/DC1
Materials and Methods
SOM Text
Figs. S1 to S3
Movie S1
References (*28*–*34*)

14 October 2011; accepted 5 January 2012
10.1126/science.1215309

Coking- and Sintering-Resistant Palladium Catalysts Achieved Through Atomic Layer Deposition

Junling Lu,[1] Baosong Fu,[2] Mayfair C. Kung,[3] Guomin Xiao,[2] Jeffrey W. Elam,[1] Harold H. Kung,[3] Peter C. Stair[4,5]*

We showed that alumina (Al_2O_3) overcoating of supported metal nanoparticles (NPs) effectively reduced deactivation by coking and sintering in high-temperature applications of heterogeneous catalysts. We overcoated palladium NPs with 45 layers of alumina through an atomic layer deposition (ALD) process that alternated exposures of the catalysts to trimethylaluminum and water at 200°C. When these catalysts were used for 1 hour in oxidative dehydrogenation of ethane to ethylene at 650°C, they were found by thermogravimetric analysis to contain less than 6% of the coke formed on the uncoated catalysts. Scanning transmission electron microscopy showed no visible morphology changes after reaction at 675°C for 28 hours. The yield of ethylene was improved on all ALD Al_2O_3 overcoated Pd catalysts.

The two main routes to the deactivation of catalysts consisting of metal nanoparticles (NPs) adsorbed on metal oxide supports are coking (the blocking of the metal surface by the accumulation of carbon on the metal) and sintering (the formation of larger metal particles, which lowers overall surface area and activity). Catalyst deactivation is costly, because catalysts must be regenerated or replaced and because processes are shut down while these steps are taken (*1*). Efforts to solve these two problems have typically focused on one or the other individually, although they often occur simultaneously.

Coke formation (or carbon deposition) during hydrocarbon reactions (*2*–*4*) is often addressed by passivating the active metal with traces of sulfur, triphenylphosphites, tin, bismuth, *et al.* (*5*–*10*); formation of an alloy (*5*, *9*–*12*); or accelerated coke removal through gasification (*9*, *13*). The sintering of metal NPs at high temperatures, particularly above the Tammann temperature (half of the bulk melting point in degrees kelvin), has been prevented in a few cases through steric stabilization by an overlayer of inorganic oxide such as mesoporous silica (*14*, *15*), tin oxide (*16*), zirconia (*17*), or ceria (*18*). In these examples, oxide shells, tens of nanometers thick, are formed around the metal NPs by chemical vapor deposition, dendrimer encapsulation, or grafting. The shell thickness is often poorly controlled, which leads to a decrease in catalytic activity from mass transfer resistance associated with shells that are thicker than desired. None of the above methods has achieved simultaneous inhibition of coking and sintering of supported metal catalysts, while maintaining high catalytic activity in high-temperature applications.

We report that Al_2O_3 overcoats, with a thickness near 8 nm, on supported Pd catalysts can effectively inhibit coke formation and greatly improve the thermal stability of Pd at temperatures

[1]Energy Systems Division, Argonne National Laboratory, Argonne, IL 60439, USA. [2]School of Chemistry and Chemical Engineering, Southeast University, Nanjing, 211189, China. [3]Department of Chemical and Biological Engineering, Northwestern University, Evanston, IL 60208–3120, USA. [4]Department of Chemistry, Northwestern University, Evanston, IL 60208,USA. [5]Chemical Science and Engineering Division, Argonne National Laboratory, Argonne, IL 60439, USA.

*To whom correspondence should be addressed. E-mail: pstair@northwestern.edu